

Comparative Study of Aluminum–Copper Dissimilar Laser Welding Simulation and Experiment

Achmad Abroori,¹ Yean-Der, Kuan,^{1,2*} and Shang-Wu Tsai³

¹Graduate Institute of Precision Manufacturing, National Chin-Yi University of Technology,
No. 57, Sec. 2, Zhongshan Rd., Taiping Dist., Taichung 411030, Taiwan (R.O.C.)

²Refrigeration, Air Conditioning, and Energy Engineering, National Chin-Yi University of Technology,
No. 57, Sec. 2, Zhongshan Rd., Taiping Dist., Taichung 411030, Taiwan (R.O.C.)

³Automotive Research and Testing Center,
No. 6, Lugong S. 7th Rd., Lukang Township, Changhua County 505004, Taiwan (R.O.C.)

(Received September 29, 2025; accepted November 7, 2025)

Keywords: aluminum, copper, dissimilar material, laser welding

In this study, we examine the relationship between the numerical simulation and experimental validation of laser welding for dissimilar aluminum–copper joints, with a focus on temperature distribution, molten pool evolution, and weld bead geometry. A finite-volume-based thermal model was established using a 1000 W laser power, a scanning speed of 275 mm/s, and a spot radius of 0.06 mm. At the same time, corresponding experiments were conducted under identical conditions to capture the cross-sectional features of the welded joint. The simulation results showed strong agreement with experimental measurements, with a mean absolute error of less than 10% across most evaluated parameters, including penetration depth and bead width. However, a localized deviation of approximately 22% was observed in the heat-affected zone boundary, which can be attributed to simplifications in thermal boundary conditions, the use of temperature-dependent material properties, and experimental measurement uncertainties. Despite these discrepancies, the developed model successfully captured the dominant heat transfer and melting mechanisms in aluminum–copper laser welding, preserving both accuracy and fidelity to the trend. The validation demonstrates that simulation provides a cost-effective and reliable predictive tool, reducing the need for extensive experimental trials while enabling process optimization in joining dissimilar metals. The findings highlight the potential of simulation-driven welding design for accelerating parameter selection, minimizing resource consumption, and improving manufacturing efficiency. Future refinements, including the incorporation of temperature-dependent thermophysical properties, calibrated absorptivity, and melt-pool convection physics, are anticipated to enhance predictive accuracy and extend the model's applicability to more complex joint geometries and variable process conditions.

*Corresponding author: e-mail: ydkuan@ncut.edu.tw
<https://doi.org/10.18494/SAM5954>

1. Introduction

Laser welding utilizes highly concentrated energy to join workpieces, providing high-quality results, precise energy control, deep penetration, high speed, and minimal heat-affected zones (HAZs). However, achieving a good weld requires the careful adjustment of parameters such as laser power and speed to optimize penetration, bead width, and weld pool geometry. Wu and co-workers reported that brittle intermetallic compounds, residual stresses, and fractures are common problems in dissimilar metal welding, reducing joint performance.⁽¹⁾ A key factor is the thickness of the intermetallic reaction layer; within limits, it ensures good mechanical properties, but excessive thickness makes the joint hard and brittle. Laser welding helps mitigate these issues through rapid melting and solidification, which suppresses excessive intermetallic formation and improves joint quality. Both theoretical and experimental studies confirm that keyhole and weld pool behaviors play a decisive role in determining welding quality in deep-penetration laser welding.

By using the numerical model for keyhole behavior in laser welding, Rai and co-workers determined the temperature and velocity fields, weld geometry, and solidification of different materials.^(2,3) However, in the assumption, the upper surface of the workpiece was flat, and the shape of the keyhole was not the actual vapor–liquid interface as this model does not consider the effect of the recoil pressure caused by metal evaporation. Their findings suggested that convection was the primary mechanism for heat transfer. Recent studies have revealed a significant increase in keyhole creation, molten pool dynamics, and welding flaws, including the development of porosity and spatter. Na and co-workers and Pang and co-workers employed a ray-tracing technique to simulate multiple laser reflections along the keyhole wall while also capturing the outline of a real-time keyhole.^(4–8) Their research revealed that the interplay of recoil pressure brought on by metal vaporization, surface tension, and hydrostatic pressure led to the development of keyholes. Additionally, the collapse of the keyhole contributed to pore creation.

In this study, we aim to compare the simulation and experimental results of laser welding and investigate fluid phenomena during melting, solidification, and weld pool geometry in the laser welding process. We utilize ANSYS Fluent software simulation and the parameter condition, which is defined using ANSYS UDF.

2. Simulation and Experimental Setup

The challenges of numerical modeling in laser welding are, in particular, the difficulty of obtaining accurate temperature-dependent thermophysical properties. Because such data are limited, most models rely on fixed or assumed values,⁽⁹⁾ as seen in the approach adopted by the DebRoy group at Penn State, where a constant laser absorption coefficient was used for pulsed laser welding.⁽¹⁰⁾ Since material properties change with temperature, modeling the heat source, material structure, and overall process becomes complex and time-consuming, further hindered by the lack of specialized modeling software. To address this problem, we developed a model database to enable faster and more reliable welding simulations.⁽¹¹⁾ We assumed that the material

properties of pure copper and pure aluminum are accurately modified to identify the crucial factors leading to irregular melting pools.⁽¹²⁾

ANSYS is adapted to simulate the plasma arc welding process through secondary development using C-based user-defined functions (UDFs). These UDFs define material properties, initialize domain settings, modify the keyhole boundary, and introduce additional momentum and energy source terms. The momentum equation is solved by the pressure implicit with the splitting of operators (PISO) method, while ANSYS Fluent handles fluid dynamics and boundary conditions. Extra energy and heat flux are applied as transient boundary conditions on the weld surface, and adaptive mesh refinement is used to track the evolution of the surface topology. The UDFs are dynamically linked with the Fluent CFD solver, enabling accurate and efficient modeling of plasma arc welding behavior.^(13–15)

2.1 Model description

Figure 1 shows the structure of our simulations and experiments on dissimilar laser welding. The geometry of the observation area is 20 mm, with a 10 mm welding length, a 0.5 mm thickness of aluminum (A1050) on the top, and a 1.0 mm thickness of copper (C1100) at the bottom.

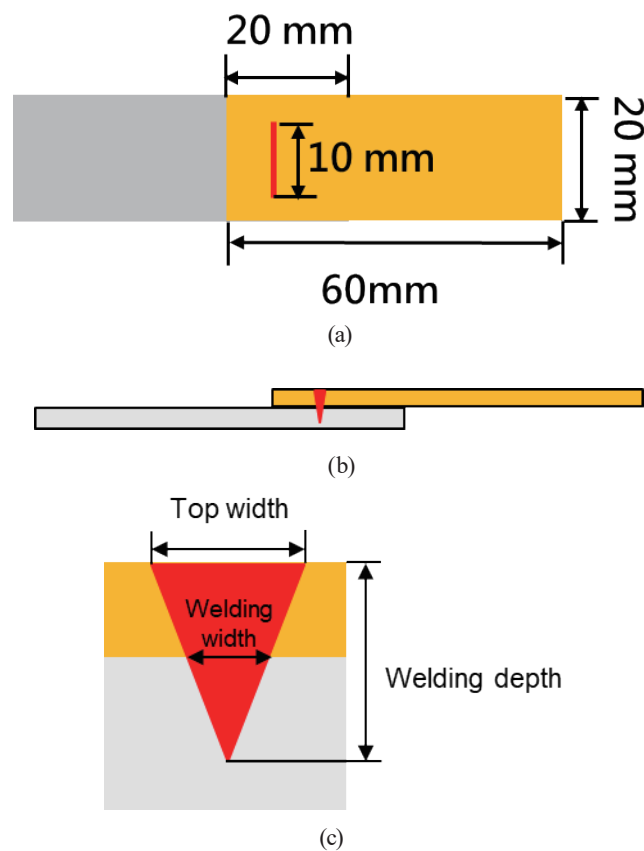


Fig. 1. (Color online) Lap welding simulation and experiment setup: (a) top view, (b) side view, and (c) detailed weld bead structure to be observed.

2.2 Mathematical model

The laser heat source model for laser welding uses the Gaussian heat source model with a circular spot and light intensity expressed as^(1,16)

$$Q(x, y, z) = \eta W / (2\pi r^2 d) \exp\left(-\left(0.6r^2\right) / R^2 - 1000Z\right), \quad (1)$$

where η is the absorption coefficient, W is the laser power, r is the surface radius, and d is the welding depth. In continuous laser welding, the radius r is expressed as

$$r = \sqrt{\left[(x - Ut)^2 + y^2\right]}, \quad (2)$$

where U is the laser scanning speed and t is time.

To perform a numerical analysis of laser welding on dissimilar metals, the mass conservation is expressed as⁽¹⁾

$$\partial / \partial t(\rho) + \nabla \cdot (\rho \vec{v}) + S_M = 0, \quad (3)$$

where ρ is the density, \vec{v} is the velocity vector, and S_M is the mass source. The momentum conservation is expressed as⁽¹⁾

$$\partial / \partial t(\vec{v}) + \vec{v} \cdot \nabla \vec{v} = -1 / \rho \nabla P + \mu \nabla^2 \vec{v} + S_m + g, \quad (4)$$

where P is the pressure, μ is the dynamic viscosity, S_m is the momentum source, and g is the gravity constant. The energy conservation is⁽¹⁾

$$\partial H / \partial t + \vec{v} \cdot \nabla H = k \nabla^2 T + S_E, \quad (5)$$

where H is the enthalpy, k is the thermal conductivity coefficient, T is the temperature, and S_E is the energy source.

2.3 Numerical method

We are solving 3D models using a commercial software package named Fluent. The mesh of the computed domain, with dimensions of $20 \times 20 \times 1.5 \text{ mm}^3$, employs a regular grid in the simulation, with a cell size of 0.05 mm. In the simulation, the species transport model accounts for the interaction between aluminum and copper phase, and the multiphase flow characteristics of the molten metal material are modeled using the volume of fluid (VOF) approach. The calculation domain, source terms, and material property are initialized in the equation definition using UDF. UDF definitions utilize the PISO method, which involves solving the pressure

correction equation twice, making it more efficient with better convergence than existing techniques.⁽¹⁾

3. Results and Discussion

This study involves simulations and experiments of aluminum–copper dissimilar metal laser welding. The simulation and experiment setup is shown in Fig. 1. At this stage, we use a 2000 W laser power source, with a scanning speed of 275 mm/s and a laser spot radius of 0.06 mm. Below, we present the results from the experiment and the simulation.

Figure 2 shows the simulated temperature distribution across the aluminum–copper joint during laser irradiation. The temperature gradient shows a sharp increase in the laser interaction zone, where the temperature exceeds the melting point of both aluminum and copper, which ensures metallurgical bonding. The heat spreads radially and vertically into the substrate, with higher concentration observed in copper owing to its higher thermal conductivity. This distribution confirms the model’s ability to reproduce anisotropic heat transfer between dissimilar metals. The experimental observation of bead morphology supports this prediction, as the fusion zone is wider on the copper side. Minor deviations can be attributed to the assumption of uniform laser absorption in the simulation, whereas in practice, reflectivity and surface roughness may vary.

Figure 3 illustrates the evolution of the molten pool over time under constant laser power and scanning speed. In both simulation and experiment, the molten pool initially exhibits a

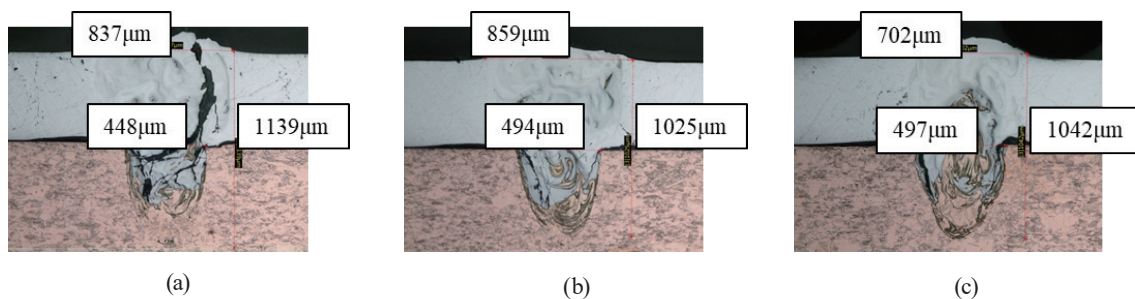


Fig. 2. (Color online) Laser welding experiment results with a 2000 W power source, 275 mm/s scanning speed, and 0.06 mm laser spot radius. (a), (b), and (c) show the results of three experiments.

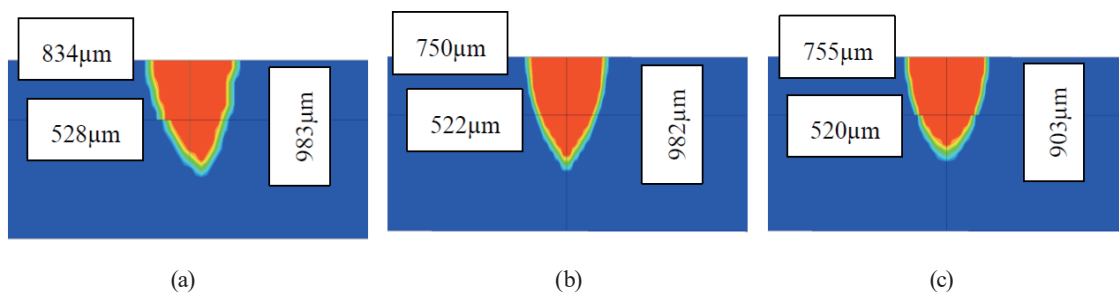


Fig. 3. (Color online) Laser welding simulation results with a 2000 W power source, 275 mm/s scanning speed, and 0.06 mm laser spot radius. (a), (b), and (c) show the results of three simulations.

Table 1

Calculated percentage error between experiment and simulation results.

Average of	Experiment result (μm)	Simulation result (μm)	Percentage error (%)
Top width	799.33	779.88	2.43
Welding width	477.67	523.44	9.58
Welding depth	1068.67	955.88	10.55

semicircular profile that elongates with increasing exposure time. The simulation successfully reproduces key features such as pool depth, top width, and the characteristic tear-drop shape observed experimentally. The predicted molten pool size agrees with the experimental data within a deviation of $<10\%$, consistent with the overall mean absolute error (*MAE*) reported. The minor discrepancies—particularly in pool boundary definition—are likely due to neglecting convection-driven flow inside the melt, which can redistribute heat and solute. Despite this, the results show that the developed model is sufficiently robust for predicting pool morphology and can guide process optimization in industrial applications.

Next, using the same setup, we change the laser power source to a 1000 W laser power source to observe the effect on weld bead formation. The results from the experiment and the simulation are given below.

The experimental results of laser welding between aluminum and copper are illustrated in Fig. 4, which shows three welds formed under identical conditions. The weld bead morphology shows consistent penetration profiles, confirming the stability of the process. Minor variations in bead geometry can be attributed to material surface conditions and localized thermal fluctuations during repeated trials.

Figure 5 shows the corresponding simulation results conducted under the same input parameters. The predicted weld pool geometry closely resembles the experimental outcome, particularly in terms of penetration depth and top bead width. This similarity demonstrates that the simulation model is capable of reproducing key welding characteristics with a high degree of fidelity.

The experimental and simulated results are summarized in Table 2. The top width, penetration depth, and HAZ dimensions are reported with their respective errors. *MAE* across all measured parameters was found to be less than 10%, indicating excellent agreement between the experiment and simulation. Such a low deviation demonstrates that the applied numerical

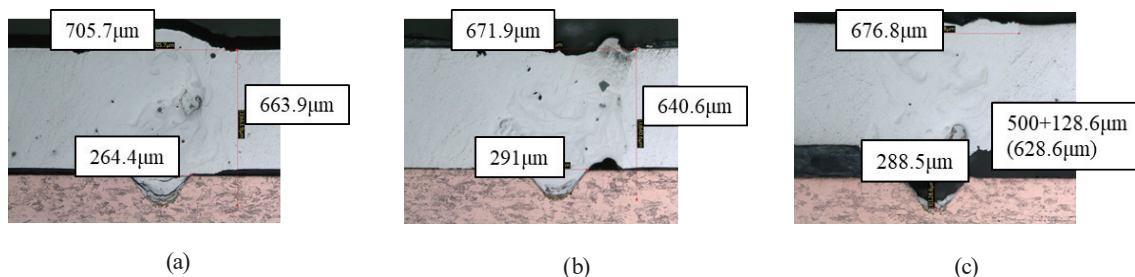


Fig. 4. (Color online) Laser welding experiment results with a 1000 W power source, 275 mm/s scanning speed, and 0.06 mm laser spot radius. (a), (b), and (c) show the results of three experiments.

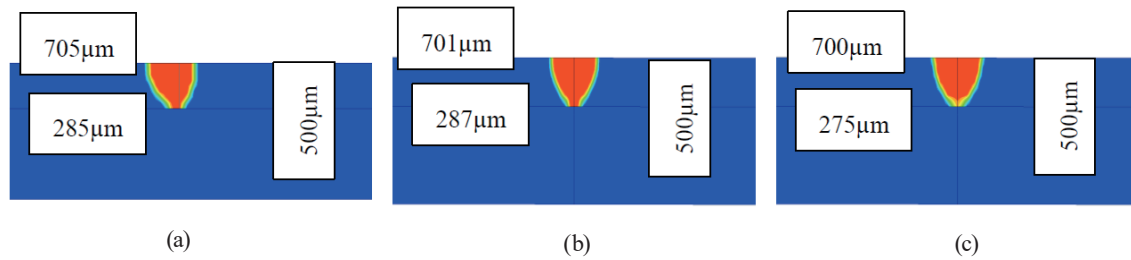


Fig. 5. (Color online) Laser welding simulation results with a 1000 W power source, 275 mm/s scanning speed, and 0.06 mm laser spot radius. (a), (b), and (c) show the results of three simulations.

Table 2

Calculated percentage error between experiment and simulation results.

Average of	Experiment result (μm)	Simulation result (μm)	Percentage error (%)
Top width	684.80	701.62	2.46
Welding width	282.80	282.50	0.11
Welding depth	644.37	500.00	22.40

model successfully reproduces the physical mechanisms of laser–material interaction, including heat conduction, melting, and solidification dynamics.

The slight differences observed—such as a differentiation of penetration depth in simulation—can be explained by simplifications in the thermal boundary conditions and the assumption of constant material properties. In reality, phase transitions, surface oxidation, and microscopic defects can alter the thermal response of the welded joint, contributing to discrepancies. However, the deviation range remains within acceptable limits for engineering applications.

Overall, the results confirm that the simulation framework can serve as a reliable predictive tool, reducing the reliance on extensive experimental trials. This contributes to cost efficiency and accelerates the optimization of process parameters for dissimilar material welding. Moreover, the close alignment of experimental and simulated data instills confidence that the model can be extended to more complex joint geometries and variable process conditions in future studies.

4. Conclusions

We presented a comparative investigation between laser welding simulation and experimental trials on aluminum–copper joints. The developed numerical model successfully reproduced the key thermal and metallurgical characteristics of the welding process, including temperature distribution, molten pool evolution, and bead geometry. The simulation results demonstrated close agreement with the experimental measurements, achieving an *MAE* of less than 10% across most parameters.

While a localized deviation of approximately 22% was observed in the HAZ boundary, this discrepancy can be attributed to simplifications in material property assumptions, thermal

boundary conditions, and the omission of certain melt-pool convection phenomena, combined with experimental measurement uncertainties. Importantly, the model preserved trend fidelity across varying process parameters, thereby confirming its predictive capability.

Overall, the findings validate the effectiveness of the proposed simulation framework as a reliable tool for optimizing processes and selecting parameters in dissimilar metal laser welding. By reducing the reliance on extensive experimental trials, the model enables the cost-effective and time-efficient development of welding strategies. Future work will focus on incorporating temperature-dependent material properties, calibrated absorptivity, and advanced melt-pool flow physics to further improve prediction accuracy and extend applicability to more complex joint geometries.

Acknowledgments

This work was supported by the Automotive Research and Testing Center, Taiwan.

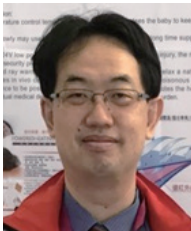
References

- 1 J. Wu, H. Zhang, Y. Feng, and B. Luo: *Metals* **8** (2018) 443. <https://doi.org/10.3390/met8060443>
- 2 R. Rai, J. W. Elmer, T. A. Palmer, and T. DebRoy: *J. Phys. D: Appl. Phys.* **40** (2007) 5753. <https://doi.org/10.1088/0022-3727/40/18/037>
- 3 R. Rai, P. Burgardt, J. O. Milewski, T. J. Lienert, and T. DebRoy: *J. Phys. D: Appl. Phys.* **42** (2008) 025503. <https://doi.org/10.1088/0022-3727/42/2/025503>
- 4 W. I. Cho, S. J. Na, C. Thomy, and F. Vollertsen: *J. Mater. Process. Technol.* **212** (2012) 262. <https://doi.org/10.1016/j.jmatprotec.2011.09.011>
- 5 J. H. Cho and S. J. Na: *J. Phys. D: Appl. Phys.* **39** (2006) 5372. <https://doi.org/10.1088/0022-3727/39/24/039>
- 6 S. Pang, L. Chen, J. Zhou, Y. Yin, and T. Chen: *J. Phys. D: Appl. Phys.* **44** (2010) 025301. <https://doi.org/10.1088/0022-3727/44/2/025301>
- 7 S. Pang, W. Chen, J. Zhou, and D. Liao: *J. Mater. Process. Technol.* **217** (2015) 131. <https://doi.org/10.1016/j.jmatprotec.2014.11.013>
- 8 S. Pang, X. Chen, J. Zhou, X. Shao, and C. Wang: *Opt. Lasers Eng.* **74** (2015) 47. <https://doi.org/10.1016/j.optlaseng.2015.05.003>
- 9 M. R. Frewin and D. A. Scott: *Welding J.* **78** (1999) 15.
- 10 J. Sabbaghzadeh, M. Azizi, and M. J. Torkamany: *Opt. Laser Technol.* **40** (2008) 289. <https://doi.org/10.1016/j.optlastec.2007.05.005>
- 11 S. He, S. Chen, Y. Zhao, N. Qi, and X. Zhan: *J. Manuf. Processes* **63** (2021) 121. <https://doi.org/10.1016/j.jmapro.2020.04.043>
- 12 The National Institute of Standards and Technology (NIST): Thermophysical properties. <https://materialsdata.nist.gov/bitstream/handle/11115/166/Thermophysical%20Properties.pdf?sequence=3&isAllowed=y> (accessed August 2025).
- 13 T. Q. Li, L. Chen, Y. Zhang, X. M. Yang, and Y. C. Lei: *Int. J. Heat Mass Transfer* **150** (2020) 119296. <https://doi.org/10.1016/j.ijheatmasstransfer.2019.119296>
- 14 L. Li, G. Peng, J. Wang, J. Gong, and S. Meng: *Int. J. Heat Mass Transfer* **133** (2019) 812. <https://doi.org/10.1016/j.ijheatmasstransfer.2018.12.165>
- 15 M. R. N. Esfahani, J. Coupland, and S. Marimuthu: *J. Mater. Process. Technol.* **224** (2015) 135. <https://doi.org/10.1016/j.jmatprotec.2015.05.005>
- 16 A. K. Unni and M. Vasudevan: *Mater. Today* **45** (2021) 4465. <https://doi.org/10.1016/j.matpr.2020.12.842>

About the Authors

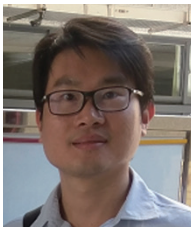


Achmad Abroori is a Ph.D. candidate of the Graduate Institute of Precision Manufacturing at National Chin-Yi University of Technology, Taichung City, Taiwan. He has been a research assistant in the Department of Refrigeration, Air Conditioning, and Energy Engineering at National Chin-Yi University of Technology, Taichung City, Taiwan, since 2020.



Yean-Der Kuan is a distinguished professor and Dean of the College of Engineering of National Chin-Yi University of Technology, Taichung City, Taiwan. He received his Ph.D. degree from the Department of Mechanical and Aerospace Engineering at the University of Missouri, USA, in 2000. Currently, he is the president of the Taiwan Society of Heating, Refrigeration and Air Conditioning, the director of the Taiwan Energy Association, the director of the Taiwan Association for Hydrogen Energy and Fuel Cells, and a member of the American Society of Heating, Refrigerating, and Air-Conditioning. His research interests include the fields of energy saving and renewable energies, and air-conditioning components and systems.

(ydkuan@ncut.edu.tw)



Shang-Wu Tsai is a computer-aided engineering (CAE) engineer at the Automotive Research & Testing Center (ARTC) in Taiwan. He received his Ph.D. degree in mechanical engineering from National Cheng Kung University, Tainan, Taiwan. His research interests are focused on fracture mechanics, finite element analysis, and structural mechanics.